



LAWRENCE
LIVERMORE
NATIONAL
LABORATORY

Event-by-event study of photon observables in spontaneous and thermal fission

R. Vogt, J. Randrup

September 28, 2012

Physical Review C

Disclaimer

This document was prepared as an account of work sponsored by an agency of the United States government. Neither the United States government nor Lawrence Livermore National Security, LLC, nor any of their employees makes any warranty, expressed or implied, or assumes any legal liability or responsibility for the accuracy, completeness, or usefulness of any information, apparatus, product, or process disclosed, or represents that its use would not infringe privately owned rights. Reference herein to any specific commercial product, process, or service by trade name, trademark, manufacturer, or otherwise does not necessarily constitute or imply its endorsement, recommendation, or favoring by the United States government or Lawrence Livermore National Security, LLC. The views and opinions of authors expressed herein do not necessarily state or reflect those of the United States government or Lawrence Livermore National Security, LLC, and shall not be used for advertising or product endorsement purposes.

Event-by-event study of photon observables in spontaneous and thermal fission

R. Vogt^{1,2} and J. Randrup³

¹*Physics Division, Lawrence Livermore National Laboratory, Livermore, CA 94551, USA*

²*Physics Department, University of California, Davis, CA 95616, USA*

³*Nuclear Science Division, Lawrence Berkeley National Laboratory, Berkeley, CA 94720, USA*

(Dated: September 27, 2012)

The event-by-event fission model **FREYA** is employed to study photon observables in spontaneous fission and fission induced by thermal neutrons. Comparison with available data is made as far as possible, including some recent correlation studies.

I. INTRODUCTION

Prompt photon emission in fission, particularly in conjunction with neutrons, is important for understanding the fission process. Photons are more sensitive to the angular momentum of the fission fragments than neutrons are and so they provide an additional means for elucidating the fission process.

The prompt photons, moving at light speed, arrive at detectors before the neutrons and can thus be separated from those by means of sufficiently fast detectors. Their contribution to the total energy deposition in fission is not well known, with only sparse information in data compilations such as ENDF-B/VII.0 [1]. However, this information is very important for applications.

Applications that go beyond simply recording the photon energy deposition include identifying nuclear material by various detection techniques. To make use of photon signals from fission in such applications, it is important to have a good phenomenological understanding of prompt photon emission from fission.

Previously, we discussed neutron observables from spontaneous and neutron-induced fission [2]. In this paper, we study photon emission with the event-by-event fission model **FREYA**. We focus on fissile isotopes where data already exist, in particular $^{235}\text{U}(n_{\text{th}},f)$ and $^{252}\text{Cf}(sf)$. In Sect. II we discuss the existing data. We then describe the implementation of photon emission in **FREYA** in Sect. III and compare our calculations to the data in Sect. IV. Next, we briefly address possible applications and finally, in Sect. VI, make our concluding remarks.

II. AVAILABLE PHOTON DATA

The data on prompt photon fission observables are rather sparse and some are relatively old. Some of the available differential data are shown in Figs. 1 and 2. Nifenecker *et al.* [3] and Nardi *et al.* [4] reported results with a $^{252}\text{Cf}(sf)$ source while Pleasonton *et al.* [5] employed thermal neutrons on ^{235}U in their experiment. There are clear inconsistencies between the above-mentioned Cf data sets, both taken in the early 1970's, likely arising from the experimental techniques as well as the assumptions employed in the analyses. We will briefly

describe these three measurements before discussing two more recent Cf measurements.

We begin with the $^{235}\text{U}(n_{\text{th}},f)$ photon measurement by Pleasonton *et al.* [5] of the average number of photons, \overline{N}_γ , and the total energy carried away by photons, \overline{E}_γ , as functions of fragment mass A and total kinetic energy, TKE. In each event they measured the kinetic energies of the two fragments and the strength of the photon signal. They also measured the time between the arrival of the fragment and photon pulses in their respective detectors to eliminate delayed fission photons and neutrons. They also made two control measurements. One measured the correlated kinetic energies of the fragments alone to control for changes in the fragment detector resolution. The other moved the target upstream of the center of the detector and rotated the detector about the center to put a limit on the number of photons originating from fragments stopped in the detectors.

The experiment was designed to make use of the fact that the isotropy of the angular distribution of photons in the center of mass frame of the fission event, $W_0(\theta) = W_0(\theta + \pi)$, is destroyed by the boost to the lab frame, $W(\theta) \neq W(\theta + \pi)$. They aligned the photon and fragment detectors coaxially to determine the number of photons emitted from individual fragments separately. The measured fragment masses and kinetic energies were corrected for prompt neutron emission to obtain the pre-neutron emission values of A and TKE using a smoothed version of the Apalin ^{235}U data on $\overline{\nu}(A)$ [6], the average neutron multiplicity as a function of A , assumed to be independent of TKE. Since they collected their data on paper tape, they had to correct for the dead time of the paper-tape punch. They used the data from the control experiment which measured fragments alone to count the number of fissions. Using this unsmoothed fragment distribution in the analysis of \overline{N}_γ and \overline{E}_γ introduces additional statistical fluctuations into their data, shown in Figs. 1 and 2.

Pleasonton *et al.* found that \overline{E}_γ and \overline{N}_γ depend on fragment mass, as shown in Fig. 1(a) and Fig. 11 respectively, as shown on the bottom of Fig. 1. Because they measured both multiplicity and energy, they also studied the ratio $\epsilon = \overline{E}_\gamma/\overline{N}_\gamma$. There is a minimum in ϵ at $A = 145$ (due to a maximum in \overline{N}_γ) which persists until $A_H \approx 132$ where \overline{N}_γ is minimal because of the reduced deformation for the doubly-magic value of A_H . They find

a sawtooth shape similar to that seen in $\overline{\nu}(A)$ but with a different location of the edge of the ‘tooth’. Rather than at $A \approx 132$ for the doubly-magic fragment mass, as is the case for $\overline{\nu}(A)$ (see *e.g.* Ref. [2]), the edge appears to be at $A \approx 110$ for $^{235}\text{U}(n, f)$, approaching the symmetry region. The average values of \overline{N}_γ and \overline{E}_γ for the light and heavy fragments are $\langle \overline{N}_\gamma \rangle_L = 3.63 \pm 0.4$, $\langle \overline{N}_\gamma \rangle_H = 2.88 \pm 0.3$, $\langle \overline{E}_\gamma \rangle_L = 3.78 \pm 0.4$ MeV, and $\langle \overline{E}_\gamma \rangle_H = 2.66 \pm 0.3$ MeV. The differences in the sawtooth shapes for neutron and photon emission suggests important neutron-photon competition. They proposed that, because photon emission is the dominant means of reducing fragment angular momentum, the lower value of $\langle \overline{E}_\gamma \rangle_H$ indicates that the heavy fragment is created with greater initial angular momentum.

Assuming that all the prompt photon emission measured by Pleasonton *et al.* is due to quadrupole transitions after neutron emission, independent of S , has ceased, $S(A) \approx 2\overline{N}_\gamma(A)$. Then $S \approx (0 - 2)\hbar$ near magic values of A and $\approx 10\hbar$ for deformed fragments, giving an average of $S \approx 6.4\hbar$ (see Fig. 11 for these data). The data are consistent with a slow decrease of \overline{E}_γ with TKE, shown in Fig. 2(a), because higher TKE is associated with lower deformations at scission, hence lower total excitation energy TXE. This is also consistent with the light fragment being more deformed with higher S for low TKE while the heavy fragment is more deformed with higher S when TKE is high. Their results are in relatively good agreement with the $^{252}\text{Cf}(\text{sf})$ measurement of Nardi *et al.* [4] but not with the conclusions of Nifenecker and *et al.* [3], as we next discuss.

Nifenecker *et al.* measured both neutrons and photons to study the competition between neutron and photon emission near the neutron separation energy [3]. They placed their Cf source and fragment detectors in the center of a spherical gadolinium-loaded liquid scintillator tank 1 m in diameter. The neutrons were distinguished from photons by timing: the photon pulse came first, followed several microseconds later by neutrons, captured by the gadolinium in the tank after slowing down. The neutrons were detected through the 8.2 MeV photon capture line. Because the prompt photon pulse includes contributions from recoil protons produced by neutrons emitted from the fragments and interacting in the material, this background must be subtracted to obtain the photon signal. The pre-neutron emission mass and kinetic energy of each fragment was deduced and the prompt energy release, the fission Q value, was determined from their data set. Their extracted experimental Q value was 1-2 MeV higher than the tabulated values of $Q(A)$ in Ref. [7].

They reported the average combined photon energy from both fragments as a function of the light fragment mass, $\overline{E}_\gamma(A_L)$, shown in Fig. 1(b), and total fragment kinetic energy, TKE, shown in Fig. 2(a). The total photon energy measured by Nifenecker *et al.* [3] increases almost linearly with A_L for $A_L > 100$, attributed to an increased dependence of photon emission on the total fragment ex-

citation energy. There is an apparent enhancement in the symmetric region, $A_L \rightarrow 126$, which may be caused by an underestimate of the neutron correction due to uncertainties in the fission neutron energy near symmetry. Nifenecker’s data as a function of A_L is compared to that as a function of single fragment mass shown in Fig. 1(a). To present the results of [4, 5] in Fig. 1(b), the energies of the fragment pairs that combine to give $A = 136$ [5] and $A = 252$ [4] are summed and their uncertainties added for direct comparison.

The strong linear decrease in \overline{E}_γ with TKE observed by Nifenecker [3] in Fig. 2(a) was attributed to neutron-photon competition. Note that the other measurements [4, 5] also show some decrease in \overline{E}_γ with TKE but it is not as strong.

Nifenecker *et al.* assert that their results may be explained by the assumption that the fragment angular momentum increases linearly with its excitation energy E^* , $\overline{S}(E^*) = aE^* + S_0$, where the ground state spin, S_0 , is A dependent. They extract $a \sim 0.2\hbar$, assuming that S changes by $2\hbar$ for every MeV of energy carried away by photon emission. This linear behavior of S with excitation energy can then account for the sawtooth-like behavior of $E_\gamma(A)$, shown in Fig. 1(a). The average total photon energy as a function of neutron multiplicity from the two fragments, shown in Fig. 2(b), is $E_\gamma = (0.75\overline{\nu} + 4)$ MeV [3], a rather striking positive correlation, if true.

Previous calculations [8] of the angular momentum acquired by fragments through mutual Coulomb excitation at scission found that, for a given fragment deformation, the angular momenta increases rapidly with TKE. This conclusion is in contradiction with Nifenecker’s result that the angular momentum increases with excitation energy rather than TKE. However, since Ref. [8] also suggested that the fragment angular momentum increases with deformation energy, Nifenecker *et al.* concluded that the fragment deformation has the dominant effect on its angular momentum. Since only part of the fragment excitation energy is due to its rotational energy, it is not at all clear that the effect can be as large as claimed in Ref. [3].

The measurements of Nardi *et al.*, shown in Figs. 1 and 2(a), used plastic scintillators which allowed a relatively straightforward determination of the total energy release due to photons because the photon energy absorbed by the scintillator is proportional to the total incident photon energy. They assume that the fraction of photon energy absorbed in the detector is independent of the energy of the prompt photons. A thin Cf source was placed inside a vacuum chamber with fragment detectors on both sides, also in the chamber. The scintillators were placed 60 cm from the source, behind the fragment detectors and outside the chamber. They separated photons from neutrons using time-of-flight techniques. Because they had a smaller geometric acceptance than Nifenecker, they were able to measure the total energy release due to photon emission from individual fragments, not pos-

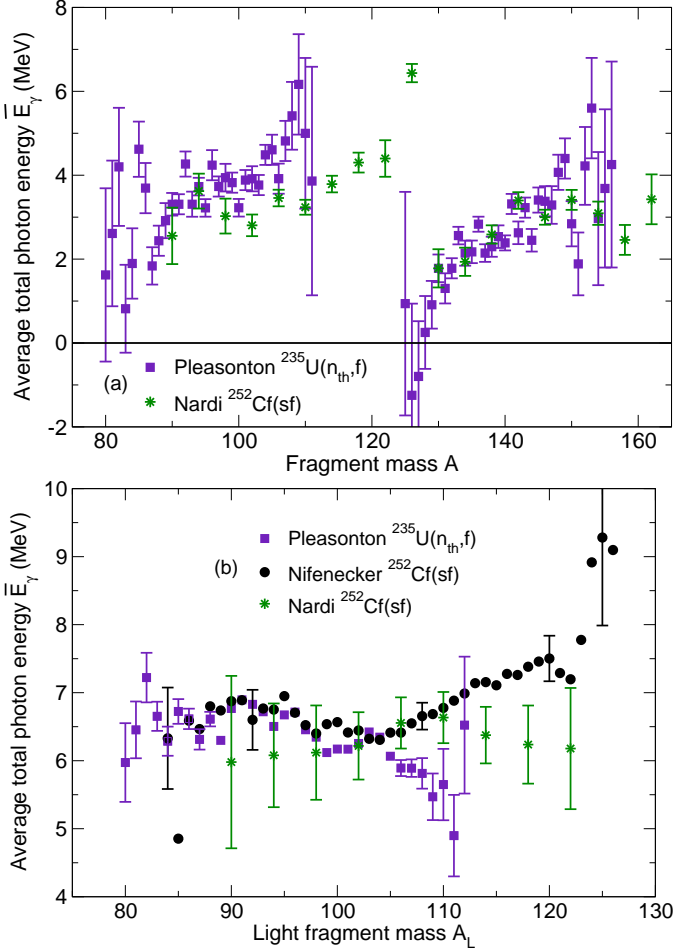


FIG. 1: (Color online) The average total emitted photon energy is shown as a function of the fragment mass, A (a) and light fragment mass, A_L (b). The data on $^{235}\text{U}(n_{th},f)$ are from Ref. [5] (■), while the data on $^{252}\text{Cf}(sf)$ are from Refs. [3] (●) and [4] (*). The data in (a) are combined pairwise to facilitate comparison with the results of Ref. [3] as a function of A_L .

sible in Nifenecker's 4π geometry. Thus Nardi reported $\bar{E}_\gamma(A)$, while Nifenecker only reported $\bar{E}_\gamma(A_L)$.

Although Nardi's average total photon energy, $\bar{E}_\gamma = 6.7 \pm 0.4$ MeV [4], is similar to Nifenecker's result, the more differential behavior exhibits substantial differences. The shape of $\bar{E}_\gamma(A)$ is similar to a sawtooth like $\bar{\nu}(A)$ but with the minimum at lower A and a less pronounced dip at the edge of the tooth, now at symmetry, $A = 126$. This result is similar to Pleasonton's $^{235}\text{U}(n,f)$ measurement albeit a weaker function of A . Nardi reported \bar{E}_γ , \bar{N}_γ and $\epsilon = \bar{E}_\gamma/\bar{N}_\gamma$. They noted that the highest values of ϵ are near the doubly-closed shell $A \approx 132$. This result, also noted by Pleasonton [5], might suggest that the smaller deformation of the heavy fragment, which reduces the probability for neutron emission, also allows fewer photons to be emitted without substantially changing their total energy.

Nardi *et al.* suggested that the behavior of $\bar{E}_\gamma(A)$

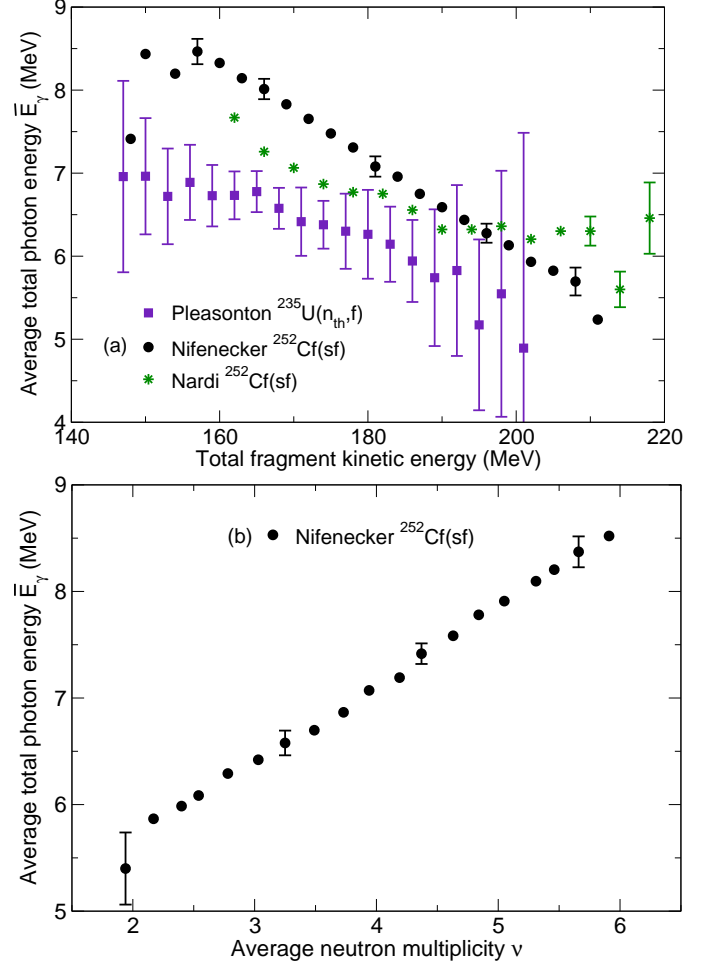


FIG. 2: (Color online) (a) The average total emitted photon energy as a function of total fragment kinetic energy for $^{235}\text{U}(n_{th},f)$ [5] (■), while the data on $^{252}\text{Cf}(sf)$ are from Refs. [3] (●) and [4] (*). (b) The average total emitted photon energy as a function of the average neutron multiplicity for $^{252}\text{Cf}(sf)$ [3] (●).

(Fig. 1) and $\bar{E}_\gamma(\text{TKE})$ (Fig. 2) is due not to fragment angular momentum (as claimed in Ref. [3]) but to the variation of neutron binding energy in the fragments. They reached this conclusion after finding good agreement between their results and a simulation of statistical neutron emission which assumed that the fragment S was unchanged by neutron emission. They thus ruled out strong variation of angular momentum with TKE (and thus TXE).

Using the tabulated reaction Q values [7], they found that every emitted neutron increases the neutron binding energy in the daughter fragment by ~ 0.26 MeV assuming that $Z(A)$ is independent of TKE. Since E_γ is about half the binding energy, E_γ increases by ~ 0.13 MeV. Earlier measurements indicated that decreasing TKE by ≈ 7 MeV increases the average neutron multiplicity by 1 [9]. Thus their empirical estimated change in E_γ with TKE is $\partial\bar{E}_\gamma/\partial\text{TKE} \approx 0.13/7 \approx 0.02$ compared to the

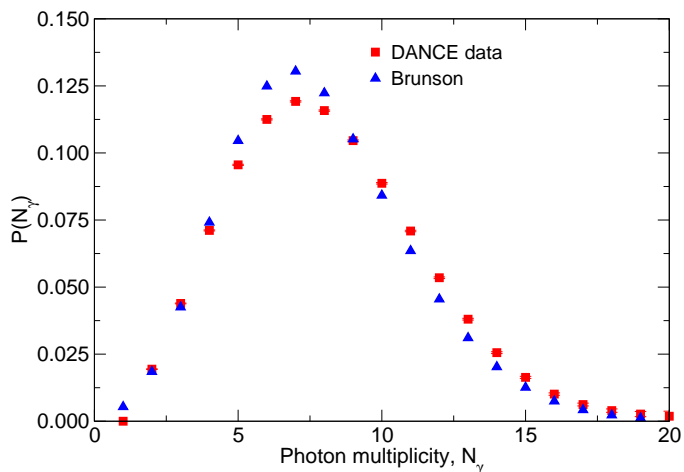


FIG. 3: (Color online) The unfolded prompt photon multiplicity distribution for $^{252}\text{Cf}(\text{sf})$ measured by DANCE (■) and the semi-empirical distribution of Brunson (▲) [11].

value of 0.036 ± 0.03 obtained from their data. The difference between their result and the phenomenological estimate places an upper limit on the magnitude of the effect of fragment angular momentum. Nardi's finding is compatible with both the earlier Cf result of Wilhelmly *et al.* [10] and the $^{235}\text{U}(n_{\text{th}}, f)$ result of Pleasonton *et al.* [5] which found S to be independent of TKE to within one unit. However, it strongly contradicts Nifenecker's result [3]. Nardi *et al.* suggested that Nifenecker's background subtraction technique to remove the recoil protons could be responsible. A new measurement, with modern detectors, of the same observables would be worthwhile.

Such new measurements are becoming available. For example, two results, from the DANCE Collaboration taking data at Los Alamos [12] and the LiBerACE Collaboration [13] making measurements at Lawrence Berkeley Laboratory, were recently published. Both are discussed briefly below.

The prompt photon energy and multiplicity distributions from $^{252}\text{Cf}(\text{sf})$ have been measured using a highly segmented 4π photon calorimeter, the Detector for Advanced Neutron Capture Experiments (DANCE) [12], together with a compact gas-filled parallel-plate avalanche counter [14]. Both the energy and multiplicity distributions were unfolded by simulating the detector response, employing a model validated by the photon calibration sources. The unfolded photon multiplicity distribution [11] is shown in Fig. 3, together with the semi-empirical distribution by Brunson [15]. They agree reasonably well.

The Livermore-Berkeley Array for Collaborative Experiments (LiBerACE) uses $^{252}\text{Cf}(\text{sf})$ to study photon multiplicity relative to neutron emission. They surrounded the Cf source with high purity germanium detectors enclosed in bismuth-germanate detectors. The geometry of the detector array provided good solid angle coverage. Room background, as well as photons from cosmic rays, were subtracted by counting photons with no

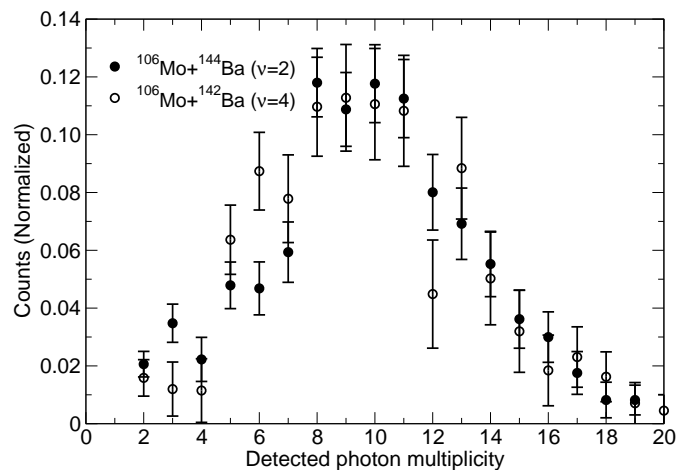


FIG. 4: (Color online) Normalized prompt photon multiplicity detected for $\nu = 2$ (●) and $\nu = 4$ (○) for the Mo+Ba fission channel resulting from spontaneous fission of ^{252}Cf [13].

source present. They made two separate analyses, one of the overall photon multiplicity and the other of the photon multiplicity correlated with neutron multiplicity.

Because the background from photons emitted by beta-decays of fission products (delayed photons) at low multiplicities was indistinguishable from prompt fission photons, only detected photon multiplicities greater than seven were used in the analysis of the overall photon multiplicity. They compared their measured multiplicity distributions to both the Brunson distribution [15] in Fig. 3 and a Monte Carlo including statistical emission of photons [16]. For $N_\gamma > 7$ the measured distribution dropped off less rapidly than Refs. [15, 16] with the Monte Carlo result [16] dropping faster with multiplicity than the Brunson determination [15].

In the second analysis, they exploited the observation of discrete energy photons coming from known transitions in identified fission products, after neutron emission, to study neutron-photon correlations. Monte Carlo calculations [2, 16] predict an anti-correlation between photons and neutrons, *i.e.* the average photon multiplicity decreases with increasing neutron multiplicity. Thus if the average photon energy is independent of neutron multiplicity, higher photon multiplicities arise from higher fragment excitation energies. On the other hand, Nifenecker *et al.* [3] suggested that there is a positive correlation between neutron and photon multiplicities, see Fig. 2(b), provided that they subtracted the neutron contribution from recoil photons correctly. This result was based on the fact that discrete photons can be separated from the background of statistical decays to the continuum and Compton scattering of high energy photons.

The LiBerACE Collaboration studied two deformed even-even product pairs: $^{106}\text{Mo}+^{144}\text{Ba}$, associated with two emitted neutrons, $\nu = 2$, and $^{106}\text{Mo}+^{142}\text{Ba}$ with $\nu = 4$. They then compared the photon multiplicity distributions from these product pairs with each other and

with Monte Carlo predictions [16]. If there is an anti-correlation between neutrons and photons, a backward shift in the centroid of the photon multiplicity distribution for four neutrons relative to two neutrons should be observed. If there is a positive correlation, the centroid for four-neutron emission should be at higher photon multiplicity than for two-neutron emission. They observed no difference in the location of the centroids for the selected Mo+Ba ratios within their significant statistical uncertainties, corresponding to no correlation between neutron and photon emission, see Fig. 4. However, it is important to remember that the Monte Carlo results are based on an average of many fragment pairs, not only specific photon transitions in selected pairs.

III. PHOTONS IN FREYA

Because the number of photons emitted as well as their spectral distributions are somewhat sensitive to the amount of angular momentum of the fission fragments, we have augmented the FREYA model [2, 17] to include fragment angular momentum.

In the scenarios considered, the initial nucleus is either in its ground state (for spontaneous fission) or it has been prepared by the absorption of a neutron of sufficiently low energy that the resulting compound nucleus has no appreciable angular momentum. Accordingly, we ignore any angular-momentum effects prior to scission, as has been the case until now.

We assume that the two fission fragments acquire some amount of angular momentum at the time of scission, \mathbf{S}_L and \mathbf{S}_H . We assume the the angular momenta of the fragments are perpendicular to the line joining their centers, thus ignoring twisting and tilting modes which are harder to excite and carry less angular momentum, so that $\mathbf{S}_f = (S_{f,x}, S_{f,y}, 0)$ for $f = L, H$. Treating the angular momenta classically for now, we sample each of the four angular-momentum components from a thermal distribution of temperature T_S , which is taken to be an adjustable parameter. This amounts to sampling S_f^2 from an exponential distribution,

$$P(S_f^2) \sim e^{-S_f^2/2\mathcal{I}_f T_S} . \quad (1)$$

where \mathcal{I}_f is the moment of inertia of the fragment f . Ref. [18] considered both a deformed rigid body, $\mathcal{I}_{\text{rigid}} = 0.4Am_N R_A^2(1 + 0.31\beta + 0.44\beta^2 + \dots)$, and an irrotational fluid, $\mathcal{I}_{\text{irrot}} = (9/8\pi)Am_N R_A^2\beta^2$ where $\beta \sim 0.3$ but adopted an intermediate value of $\mathcal{I} \sim 0.5\mathcal{I}_{\text{rigid}}$. We make a similar choice and use half the rigid value, $\mathcal{I}_f = \frac{1}{5}m_N r_0^2 A^{5/3}$.

Once the angular momenta have been selected, the associated amount of rotational energy is readily obtained,

$$E_{\text{rot}} = \frac{\hbar^2 S_L^2}{2\mathcal{I}_L} + \frac{\hbar^2 S_H^2}{2\mathcal{I}_H} , \quad (2)$$

and the energy available for statistical excitation of the fragment is reduced correspondingly.

The modified FREYA procedure is then as follows. The fragment masses and charges, (A_L, Z_L) and (A_H, Z_H) , are sampled as before and the corresponding available energy Q_{LH} is then obtained. This energy comprises not only the translational kinetic energies of the fragments and their statistical excitation energies, but now also their rotational energies. (Possible fragment distortions are not considered explicitly but their effect is included by means a subsequent energy redistribution governed by the model parameter x .) Thus, once the average total fragment kinetic energy, $\overline{\text{TKE}}$, has been sampled as before, the average combined statistical excitation energy of the fragments follows from energy conservation,

$$\overline{\text{TXE}} = \overline{E}_L^* + \overline{E}_H^* \doteq Q - \overline{\text{TKE}} - E_{\text{rot}} . \quad (3)$$

The first relation indicates that the total statistical excitation, $\overline{\text{TXE}}$, is partitioned between the two fragments. As is common, we assume that the fragment level densities are of simple Fermi-gas form, $\rho_f(E_f^*) \sim \exp(2\sqrt{a_f U_f})$, where U_f is the effective statistical energy in the fragment and a_f is the level-density parameter. We follow the prescription of Ref. [19] with the value of the asymptotic level density parameter e_0 obtained from the ^{239}Pu evaluation, assuming it to be universal.

If the two fragments are in mutual thermal equilibrium, their temperatures are equal, $T_L = T_H$, and their statistical energy will be proportional to the level-density parameters, *i.e.* $\overline{E}_f^* \sim a_f$. FREYA first assigns tentative average excitations based on such an equipartition,

$$\dot{E}_f^* = \frac{a_f(\tilde{E}_f^*)}{a_L(\tilde{E}_L^*) + a_H(\tilde{E}_H^*)} \overline{\text{TXE}} , \quad f = L, H . \quad (4)$$

where $\tilde{E}_f^* = (A_f/A_0)\overline{\text{TXE}}$. Subsequently, because the observed neutron multiplicities suggest that the light fragments tends to be disproportionately excited (probably in large part because they tend to be distorted more at scission), the average values are adjusted in favor of the light fragment,

$$\overline{E}_L^* = x\dot{E}_L^* , \quad \overline{E}_H^* = \overline{\text{TKE}} - \overline{E}_L^* , \quad (5)$$

where x is an adjustable model parameter expected be larger than unity.

After the mean excitation energies have been assigned, FREYA considers the effect of thermal fluctuations. The fragment temperature T_f is obtained from $\overline{U}_f \equiv U_f(\tilde{E}_f^*) = a_f T_f^2$, where $U(E^*) = E^*$ in the simple (unshifted) scenario. The associated variance in the excitation E_f^* is then $\sigma_f^2 = 2\overline{U}_f T_f$. Therefore, for each of the two fragments, we sample a thermal energy fluctuation δE_f^* from a normal distribution of variance σ_f^2 and modify the fragment excitations accordingly, so that

$$E_f^* = \overline{E}_f^* + \delta E_f^* , \quad f = L, H . \quad (6)$$

Energy conservation causes a compensating opposite fluctuation in the total kinetic energy leading to $\text{TKE} = \overline{\text{TKE}} - \delta E_L^* - \delta E_H^*$ [19].

The subsequent neutron evaporation occurs after the fragments have reached their asymptotic velocities and is performed as earlier: For a given fragment of statistical excitation E^* , the maximum temperature in its evaporation daughter, T_{\max} , is obtained from $aT_{\max}^2 = E^* - S_n$, where S_n is the neutron separation energy, and the neutron kinetic energy E is then sampled from

$$f_n(E) \equiv \frac{1}{N_n} \frac{dN_n}{dE} \sim E e^{-E/T_f^{\max}}, \quad (7)$$

as is easily done by letting $E = -T_{\max} \ln(\eta_1 \eta_2)$, where η_i are random numbers distributed uniformly within the unit interval $(0, 1]$. It is assumed that the emitted neutron carries no angular momentum, so the fragment angular momentum remains unaffected during the evaporation chain. For each of the two fragments, the evaporation procedure is repeated as long as the Q value for neutron emission exceeds a specified value, $E_{n,\text{cut}}$, which governs where photon emission takes over from neutron evaporation (see below).

After neutron evaporation has ceased, the residual product nucleus has a statistical excitation energy of $E^* < S_n + E_{n,\text{cut}}$. It now proceeds to de-excite by sequential photon emission which is assumed to occur in two stages: first the statistical excitation energy is radiated away by sequential photon emission, leaving a cold but rotating product nucleus which then completes its de-excitation by photon emission along the yrast line.

The statistical photon emission is treated in a manner analogous to neutron evaporation, but there are two important technical differences: there is no separation energy for photons and, because they are massless, there is no obvious end to the photon emission chain. We therefore introduce an infrared cut-off value. Furthermore, whereas the neutrons may be treated by non-relativistic kinematics, the photons are ultra-relativistic and, consequently, their phase space has an extra energy factor,

$$f_\gamma(E) \equiv \frac{1}{N_\gamma} \frac{dN_\gamma}{dE} \sim E^2 e^{-E/T}. \quad (8)$$

Here T is the nuclear temperature prior to emission which is equal to the maximum possible temperature after emission (corresponding to the emission of an extremely soft photon). The photon energy is sampled according to $E = -T \ln(\eta_1 \eta_2 \eta_3)$, where η_i are random numbers distributed uniformly within the unit interval $(0, 1]$. The photons are emitted isotropically in the frame of the emitter nucleus and the appropriate Lorentz boosts are then performed.

The above procedure is repeated until the available statistical excitation energy has been exhausted. We then dispose of the angular momentum by simulating a stretched E2 cascade. Thus, as long as $S > 2$, the angular momentum will be reduced by two units and a photon is emitted with energy $E = \frac{1}{2}[S^2 - (S-2)^2]\hbar^2/\mathcal{I} = 2(S-1)\hbar^2/\mathcal{I}$. At the end of the cascade, when $S < 2$, the remaining excitation energy is carried away by a single

T_S (MeV)	0.20	0.35	0.75	1.35	2.75
\overline{S}_f (\hbar)	2.97	3.93	5.76	7.72	11.0

TABLE I: The average magnitude of the fragment angular momentum obtained with the values of T_S employed here assuming $\mathcal{I} = 0.5\mathcal{I}_{\text{rigid}}$.

final photon. This approximate procedure can clearly be refined, but we prefer to first explore its utility before complicating the treatment.

IV. PHOTON OBSERVABLES

The photon observables are sensitive not only to the existing FREYA parameters: $d\text{TKE}$, e_0 , and x employed in our previous work [2, 17, 19], but also to the fragment “spin temperature”, T_S , the energy at which photon emission begins to dominate over neutron emission, $E_{n,\text{cut}}$, and the photon detection threshold, E_{det} .

The parameter T_S governs the magnitude of the fragment angular momentum, $\langle S_f^2 \rangle = 2\mathcal{I}_f T_S = \overline{S}_f^2$. Table I shows the mean magnitudes, \overline{S}_f , averaged over the fragment mass distribution, obtained for the values of T_S employed in this study.

We have set the detection threshold in our calculations to 150 keV, the threshold given in the recent photon multiplicity measurement in Ref. [11]. Because raising or lowering E_{det} decreases or increases the number of soft photons registered, modifying E_{det} strongly affects the photon multiplicity but has only a modest effect on the total photon energy.

Since the competition between photons and neutrons has been approximated by changing the ratio $\Gamma_n/(\Gamma_n + \Gamma_\gamma)$ from one to zero abruptly at $E_{n,\text{cut}}$, we vary the relative neutron to photon dominance by adjusting $E_{n,\text{cut}}$. We use a default minimum $E_{n,\text{cut}}$ value of 0.01 MeV (to avoid numerical problems with very low kinetic energy neutrons) and study the effect of increasing $E_{n,\text{cut}}$ on both neutron and photon observables.

We keep e_0 and x fixed to the values of our previous results, $e_0 \approx 10$ MeV and $x = 1.3$ for $^{252}\text{Cf}(\text{sf})$ ($x = 1.2$ for $^{235}\text{U}(n_{\text{th}}, \text{f})$) and study the sensitivity of the photon observables to $E_{n,\text{cut}}$ and T_S . The shift in total fragment kinetic energy, $d\text{TKE}$, is adjusted to maintain agreement with the average neutron multiplicity for the values of $E_{n,\text{cut}}$ and T_S employed. We note that the value of $d\text{TKE}$ necessary to recover $\overline{\nu}$ decreases with increasing T_S . Indeed, $d\text{TKE} \approx 0$ for ^{252}Cf with $T_S = 1.35$ MeV.

In the remainder of this section, we compare our results to the data discussed in Section II. We then go on to discuss photon-neutron correlations and the sensitivity of the neutron results to the photon parameters.

A. Average photon multiplicity

We begin by comparing our FREYA calculations to the recent DANCE prompt photon multiplicity distribution reported in Ref. [11]. The top panel of Fig. 5 compares the DANCE result to a FREYA calculation using the value $T_S = 0.35$ MeV which yields the best agreement with the measured average photon multiplicity, $\langle \bar{N}_\gamma \rangle = 8.14$. While the average multiplicity is the same in the two cases, the calculated multiplicity dispersion, $\sigma_{\bar{N}_\gamma} \approx 9.5$, is smaller than the measured value of 11.1. For reference, we also show the Poisson distribution having the same mean multiplicity as the calculation. It is evident that both the calculated and the measured distributions are broader than a Poisson, the opposite of the situation for the neutron multiplicity distribution. The semi-empirical result of Brunson [15], shown in Fig. 3, is shifted to lower multiplicity and has a narrower width compared to the DANCE data. While the narrower width is more similar to the FREYA simulation, it would be difficult to realize a lower multiplicity that is consistent with the relatively large average angular momenta obtained in earlier experiments [3, 4, 10].

While the calculation gives the right average photon multiplicity, the average angular momentum obtained with $T_S = 0.35$ MeV, namely $\bar{S} = 3.9\hbar$, is considerably smaller than that reported in earlier measurements. Therefore, we studied the sensitivity of the calculated multiplicity distribution to both the value of T_S and the neutron energy at which photon emission should begin to dominate, $E_{n,\text{cut}}$. As stated previously, the default value of $E_{n,\text{cut}}$ is 0.01 MeV. An increase of $E_{n,\text{cut}}$ will reduce the neutron emission while enhancing the photon emission, with regard to both multiplicity and energy, as discussed later.

The middle panel of Fig. 5 shows the effect of varying T_S while keeping $E_{n,\text{cut}}$ fixed. The lowest value of T_S , 0.20 MeV, while underestimating the total multiplicity, agrees best with the low- N_γ part of the distribution. Increasing T_S essentially increases the maximum average fragment angular momentum from $2.9\hbar$ with $T_S = 0.20$ MeV to $11.4\hbar$ for $T_S = 2.75$ MeV, see Table I. The corresponding average photon multiplicity increases from 7.76 to 8.78, see Table II. Keeping $E_{n,\text{cut}}$ fixed while varying T_S leaves the neutron observables unchanged as long as the parameter $d\text{TKE}$ is adjusted to maintain agreement with $\bar{\nu}$. The additional energy that goes into rotational energy with increased T_S both increases \bar{N}_γ significantly and also increases \bar{E}_γ . Thus, as we show shortly, though the agreement with the more recent multiplicity measurement is degraded, the increased average photon energy is in better agreement with the earlier measurements.

In the bottom panel of Fig. 5, T_S is kept fixed while $E_{n,\text{cut}}$ is increased from 0.01 MeV to 1.00 MeV. We have chosen the low value of $T_S = 0.20$ MeV for the comparison because it was already seen that larger values of T_S would increase the photon multiplicity beyond that supported by recent data. While such a large value of

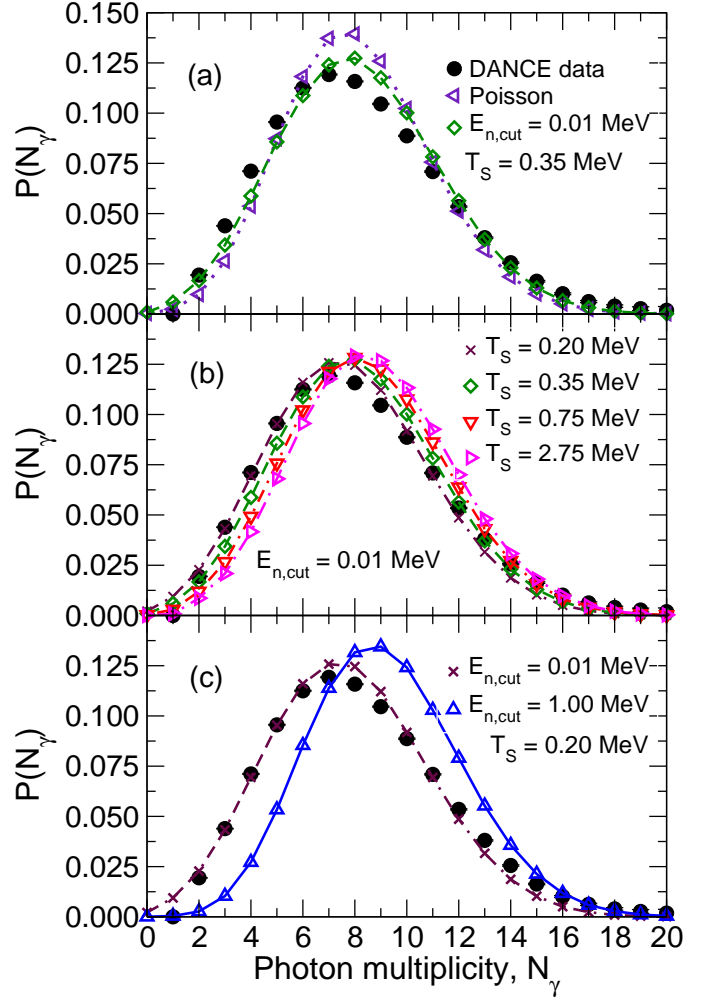


FIG. 5: (Color online) The photon multiplicity data from DANCE [12] (\bullet) are compared to FREYA calculations. (a) Calculations with $E_{n,\text{cut}} = 0.01$ MeV and $T_S = 0.35$ MeV (\diamond) are compared to a Poisson distribution with the same value of $\langle \bar{N}_\gamma \rangle$ (\triangleleft). (b) Results for fixed $E_{n,\text{cut}} = 0.01$ MeV are shown for $T_S = 0.20$ (\times); 0.35 (\diamond); 0.75 (∇); and 2.75 (\triangleright) MeV. (c) Results with fixed $T_S = 0.20$ MeV are shown for $E_{n,\text{cut}} = 0.01$ (\times) and 1.00 (\triangle) MeV.

$E_{n,\text{cut}}$ can still be brought to agree with $\bar{\nu}$ by adjusting $d\text{TKE}$, the neutron observables are affected by the higher T_S value (see Sect. IV D).

Finally, to test the sensitivity of the results to the moment of inertia, we take $\mathcal{I} = \mathcal{I}_{\text{rigid}}$ instead of $0.5\mathcal{I}_{\text{rigid}}$. In this case, the best agreement with the DANCE multiplicity, $\bar{N}_\gamma \approx 8.17$, is obtained with $T_S = 0.5$ MeV which corresponds to the increased angular momentum of $6.6\hbar$. By the time T_S has been increased to 1.35 MeV, we obtain $\bar{S} \approx 11\hbar$ and $\bar{N}_\gamma \approx 8.6$. Using the larger moment of inertia does not change the value of $d\text{TKE}$ needed to give the correct value of the average neutron multiplicity, only the angular momentum. In addition, increasing the value of \mathcal{I} does not increase the average total photon energy emitted.

T_S (MeV)	$E_{n,\text{cut}}$ (MeV)	$\langle \overline{N}_\gamma \rangle$	$\sigma_{\overline{N}_\gamma}$
$^{252}\text{Cf}(\text{sf})$			
0.20	1.00	9.219	8.553
0.20	0.01	7.760	9.525
0.35	0.01	8.143	9.496
0.75	0.01	8.494	9.358
1.35	0.01	8.655	9.223
2.75	0.01	8.779	9.162
$^{235}\text{U}(n_{\text{th}},\text{f})$			
0.20	1.00	8.758	7.886
0.35	0.01	7.752	8.721
2.75	0.01	8.388	8.345

TABLE II: The average photon multiplicity, $\langle \overline{N}_\gamma \rangle$, and the width of the multiplicity distribution, $\sigma_{\overline{N}_\gamma}$, for the values of $E_{n,\text{cut}}$ and T_S considered. Results are shown for both $^{252}\text{Cf}(\text{sf})$ and $^{235}\text{U}(n_{\text{th}},\text{f})$.

B. Photon energy and number distributions

We now consider the dependence of the $^{252}\text{Cf}(\text{sf})$ and $^{235}\text{U}(n_{\text{th}},\text{f})$ observables on fragment mass and total kinetic energy. We first focus on spontaneous fission and then turn to neutron-induced fission.

1. Spontaneous fission: $^{252}\text{Cf}(\text{sf})$

We first compare our FREYA results to the measured mass dependence of the average total photon energy released in the spontaneous fission of ^{252}Cf . In general, we find that the values of T_S that lead to agreement with the recent measurement of \overline{N}_γ , with a correspondingly low average fragment angular momentum, are not in good agreement with the earlier measurements of the photon energy observables.

This is illustrated in Fig. 6 which compares the FREYA results to the Nardi data [4]. There is a sharp drop in the measured average photon energy at symmetry, $A = 126$, that is not reproduced by the calculations. As discussed in Sect. II, the ‘sawtooth-like’ behavior of $\overline{E}_\gamma(A)$ differs from that of $\overline{\nu}(A)$ in the location of the edge of the tooth: the dip corresponds to mass-symmetric fission fragments rather than the location of the doubly-closed shell at $A \approx 132$. The FREYA results for $E_\gamma(A)$ follow the calculated behavior of $\overline{\nu}(A)$ with a decrease in the simulated photon energy at $A \approx 132$.

While the statistics are rather poor, we see that the results for $T_S = 0.35$ and 0.75 MeV are, on average, too low to reproduce the trends of the data, whereas the other three calculations do a better job. We note that while the results for $T_S = 2.75$ and $T_S = 0.2$ MeV are rather similar for the light fragment, they differ for the heavy fragment. This is likely due to the use of $x = 1.3$ which gives more of the excitation energy to the light fragment

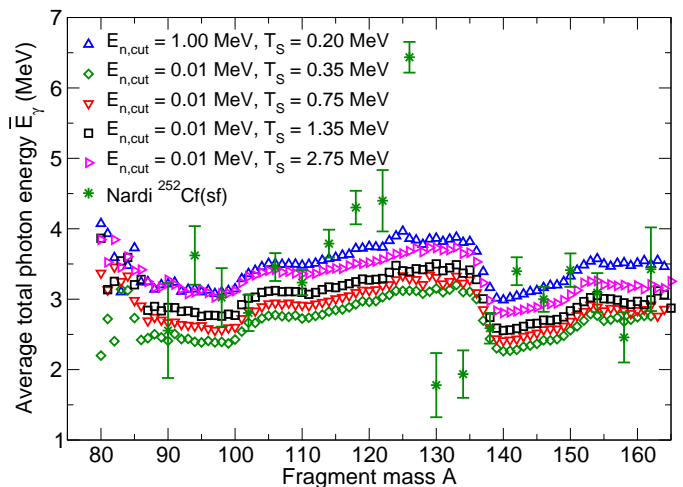


FIG. 6: (Color online) The average total photon energy as a function of fragment mass A compared to data (*) from Ref. [4]. The calculations are $E_{n,\text{cut}} = 1$ MeV, $T_S = 0.20$ MeV (\triangle) and, with $E_{n,\text{cut}} = 0.01$ MeV, $T_S = 0.35$ MeV (\diamond), 0.75 MeV (∇), 1.35 MeV (\square), and 2.75 MeV (\triangleright).

and correspondingly less to the heavy fragment. The use of $E_{n,\text{cut}} = 1$ MeV therefore effectively returns some of the excitation energy to the heavy fragment, allowing it to give proportionally more of its excitation energy to photon emission.

On the other hand, when the $\overline{E}_\gamma(A)$ data are combined to present the results as a function of light fragment mass, evidence of the structure of $\overline{E}_\gamma(A)$ is lost and the Nardi data [4] appear to be practically independent of A_L , within the large uncertainties, with the exception of the symmetric point, off the scale of the y -axis in Fig. 7. This behavior is, as already noted, in contrast to the more gradual increase in E_γ with A_L for $A_L > 108$ reported by Nifenecker [3].

The FREYA results are relatively independent of A_L except in the range $112 < A_L < 120$, corresponding to the dip near the closed shell in Fig. 6. Again the larger values of T_S for fixed $E_{n,\text{cut}}$ give better agreement with the trend of the data. Note that the two sets of data are not consistent with each other as symmetry is approached, even within the large uncertainties of Ref. [4].

The conflict between the T_S values required to reproduce the DANCE average photon multiplicity and the earlier data on $\overline{E}_\gamma(A)$ is not easily reconciled. A possible calculational solution of increasing the parameter e_0 from ≈ 10 to ≈ 14 MeV (and thereby increasing the fragment temperature) actually results in a significantly narrower multiplicity distribution, opposite the trend of the DANCE measurement, although taking $T_S = 2.75$ MeV with both values of e_0 gives a lower average multiplicity for the higher e_0 , closer to the measured average.

The TKE dependencies of the different data sets are also difficult to reconcile. Although data sets show a decrease of \overline{E}_γ with TKE, the trend is stronger in the Nardi data [4] which starts out lower and becomes almost

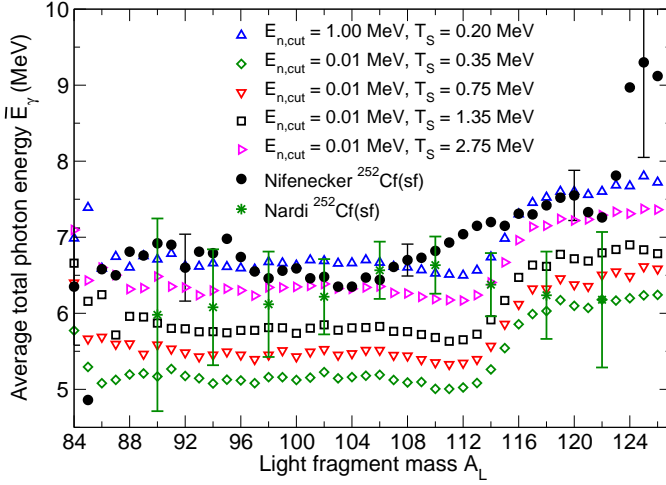


FIG. 7: (Color online) The average total photon energy as a function of light fragment mass A_L compared to data from Ref. [3] (\bullet) and Ref. [4] (\ast). The calculations are $E_{n,\text{cut}} = 1$ MeV, $T_S = 0.20$ MeV (\triangle) and, with $E_{n,\text{cut}} = 0.01$ MeV, $T_S = 0.35$ MeV (\diamond), 0.75 MeV (∇), 1.35 MeV (\square), and 2.75 MeV (\triangleright).

independent of TKE for $\text{TKE} > 180$ MeV. The FREYA result with $E_{n,\text{cut}} = 0.01$ MeV and $T_S = 2.75$ MeV is in relatively good agreement with the Nardi data in this region of TKE. But the linear decrease of the Nifenecker data [3] over the range of TKE agrees with neither the Nardi data nor FREYA. A new measurement of $\overline{E}_\gamma(A)$ and $\overline{E}_\gamma(\text{TKE})$ would be very helpful for resolving these mutual discrepancies in the data.

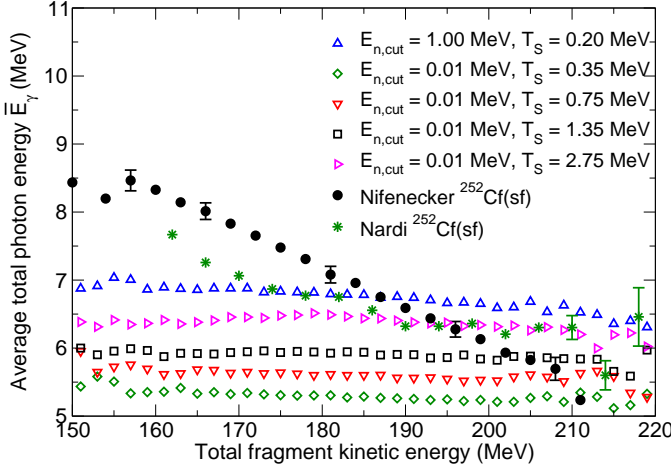


FIG. 8: (Color online) The average total photon energy emitted in a fission event as a function of the total fragment kinetic energy in the event compared to the data from Refs. [3] (\bullet) and [4] (\ast). The calculations are $E_{n,\text{cut}} = 1$ MeV, $T_S = 0.20$ MeV (\triangle) and, with $E_{n,\text{cut}} = 0.01$ MeV, $T_S = 0.35$ MeV (\diamond), 0.75 MeV (∇), 1.35 MeV (\square), and 2.75 MeV (\triangleright).

The average neutron multiplicity decreases almost linearly with TKE, as shown in Fig. 9. In this case,

FREYA agrees very well with the Budtz-Jørgensen data [20] which is averaged both over fragment yield as well as energy, while the Bowman data [21] are only averaged over energy. (They did not report mass yields.) If the photon behavior follows that of the neutrons, as suggested by Nifenecker [3], then the behavior of the photon data in Fig. 8 would be similar to this result. However, if there is an anti-correlation between neutrons and photons, or no correlation at all, as suggested by the LiBER-ACE data, then there is no reason to expect the photon energy to decrease with TKE.

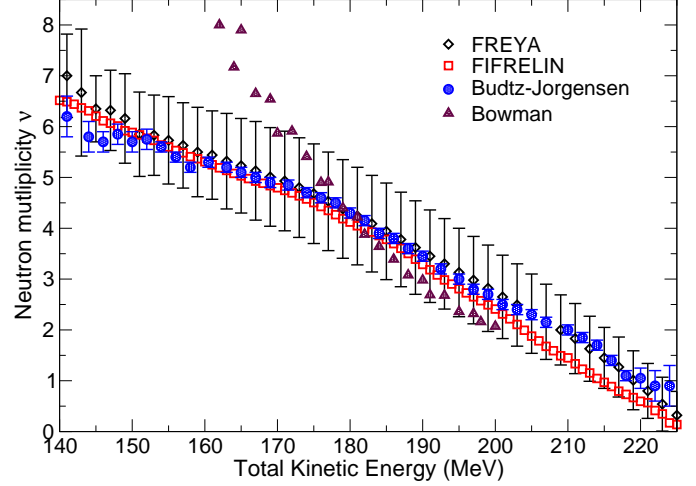


FIG. 9: (Color online) The average neutron multiplicity as a function of fragment total kinetic energy in the spontaneous fission of ^{252}Cf measured by Budtz-Jørgensen [20] (\bullet) and Bowman [21] (\blacktriangle) compared to the FIFRELIN Monte Carlo results [18] (\square) and the present FREYA calculations (\diamond), for which the vertical bars show the calculated width of the multiplicity distribution, $\bar{\nu} \pm \sigma_\nu$.

2. Neutron-induced fission: $^{235}\text{U}(n_{\text{th}}, f)$

Using the same FREYA parameter values as for the above analysis of data on spontaneous fission, we now consider the Pleasonton data on $^{235}\text{U}(n_{\text{th}}, f)$ [5]. Thus we use $T_S = 0.35$ MeV or 2.75 MeV with $E_{n,\text{cut}} = 0.01$ MeV to bracket the range of values that agree with the photon multiplicity distribution and the photon energy observables, respectively. We also use $T_S = 0.2$ MeV with $E_{n,\text{cut}} = 1$ MeV.

The results for $\overline{E}_\gamma(A)$ and $\overline{N}_\gamma(A)$ are shown with the Pleasonton data in Figs. 10 and 11. The trends of the \overline{E}_γ and \overline{N}_γ data are similar: There is a general increase for $80 < A < 110$ and also for $126 < A < 155$, although $\overline{N}_\gamma(A)$ appears to have a somewhat more linear dependence. The values of \overline{N}_γ and \overline{E}_γ (in MeV) are also very similar. The averages reported in Ref. [5] are listed in Table III together with the calculated results for the three cases displayed in Figs. 10-12.

T_S (MeV)	$E_{n,\text{cut}}$ (MeV)	$\langle \overline{E}_\gamma \rangle_L$ (MeV)	$\langle \overline{N}_\gamma \rangle_L$	$\langle \overline{E}_\gamma \rangle_H$ (MeV)	$\langle \overline{N}_\gamma \rangle_H$	$\langle \overline{E}_\gamma \rangle$ (MeV)	$\langle \overline{N}_\gamma \rangle$
Ref. [5]		3.78 ± 0.4	3.63 ± 0.4	2.66 ± 0.3	2.88 ± 0.3	6.44 ± 0.4	6.56 ± 0.3
0.20	1.00	3.3 ± 2.4	4.4 ± 1.9	3.4 ± 2.6	4.6 ± 2.0	6.4 ± 5.5	8.6 ± 2.8
				3.2 ± 2.5			
0.35	0.01	2.6 ± 1.9	3.9 ± 2.0	2.7 ± 2.0	4.0 ± 2.1	5.1 ± 4.4	7.8 ± 2.9
				2.5 ± 2.0			
2.75	0.01	3.3 ± 2.6	4.2 ± 2.0	3.3 ± 2.5	4.4 ± 2.0	6.2 ± 5.4	8.3 ± 2.8
				3.0 ± 2.4			

TABLE III: The average photon multiplicity and total energy emitted as photons in the light and heavy fragments as well as from both fragments combined. The first line shows the results extracted from the data on $^{235}\text{U}(n_{\text{th}}, f)$ [5]. The calculated result for an observable X is given as $\langle X \rangle \pm \sigma_X$, where dispersion σ_X is the *width* of the distribution of X (not the numerical error which is negligible). The values of $\langle \overline{E}_\gamma \rangle_L$ and $\langle \overline{N}_\gamma \rangle_L$ were extracted for the measured range, $80 \leq A_L \leq 110$, while $\langle \overline{N}_\gamma \rangle_L$ was extracted for the measured range $126 \leq A_H \leq 156$. However, $\langle \overline{E}_\gamma \rangle_H$ is given for both the full reported range, $126 \leq A_H \leq 156$, and $136 \leq A_H \leq 156$ (see text).

It appears that the differences between the calculated results and the data for the total photon energy and the photon multiplicity are larger than the reported error bars could accommodate. However, the calculated energy and multiplicity distributions are rather broad (their dispersions are shown in Table III), broader than the corresponding neutron distributions [2]. The ratio $\langle \overline{E}_\gamma \rangle / \langle \overline{N}_\gamma \rangle$, where the average is taken over all masses, is reported as 0.98 MeV [5], while the calculated ratio is ≈ 0.65 for $T_S = 0.35$ MeV and ≈ 0.75 for the other two cases. In addition, the calculated average energies are almost the same for the light and heavy fragments, while Ref. [5] reports $\langle \overline{E}_\gamma \rangle_H / \langle \overline{E}_\gamma \rangle_L = 0.70$. The calculated average photon multiplicities exhibit the same feature, while experimentally $\langle \overline{N}_\gamma \rangle_H / \langle \overline{N}_\gamma \rangle_L = 0.78$ [5].

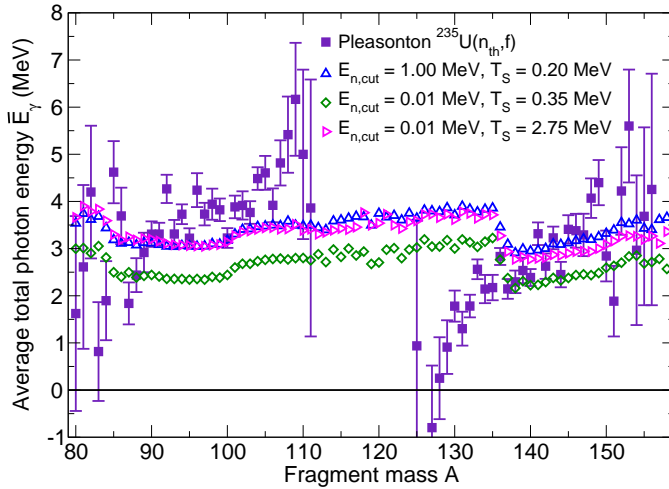


FIG. 10: (Color online) The average total photon energy as a function of fragment mass compared to the data on thermal neutron-induced fission of ^{235}U [5] (■). The calculations are $E_{n,\text{cut}} = 1$ MeV, $T_S = 0.20$ MeV (\triangle) and, with $E_{n,\text{cut}} = 0.01$ MeV, $T_S = 0.35$ MeV (\diamond) and 2.75 MeV (\triangleright).

Because of the change in slope near the closed shell at $A_H = 132$, two values of $\langle \overline{E}_\gamma \rangle_H$ are shown in Table III.

The first, $126 < A_H < 156$, matches the range of the data, while the second, $136 < A_H < 156$, excludes the region with the change of slope. Taking the narrower definition of A_H does not have a large effect on $\langle \overline{E}_\gamma \rangle_H$, but results in $\langle \overline{E}_\gamma \rangle_H / \langle \overline{E}_\gamma \rangle_L < 1$.

The calculated $\overline{N}_\gamma(A)$ is almost constant which is very different from the trend exhibited by the data. The changes in $\overline{N}_\gamma(A)$ for different values of T_S and $E_{n,\text{cut}}$ are smaller than those in $\overline{E}_\gamma(A)$.

In these calculations, we have used the same detector threshold, $E_{\text{det}} = 0.15$ MeV, as for the DANCE detector, because the threshold in the Pleasonton measurements is not clear. As stated previously, changing E_{det} does not have a significant effect on \overline{E}_γ because $E_{\text{det}} \ll \langle \overline{E}_\gamma \rangle$. However, a change in E_{det} has a stronger effect on $\langle \overline{N}_\gamma \rangle$. For example, changing E_{det} from 0.15 MeV to 0.2 MeV reduces $\langle \overline{E}_\gamma \rangle$ by $\approx 4\%$ while reducing $\langle \overline{N}_\gamma \rangle$ by $\approx 12\%$ for $T_S = 0.35$ MeV. As noted already, $\langle \overline{E}_\gamma \rangle \approx \langle \overline{N}_\gamma \rangle$ MeV for $E_{\text{det}} = 0.3$ MeV, so the calculated balance between \overline{N}_γ and \overline{E}_γ is sensitive to the employed cutoff. On the other hand, a change of the detector threshold does not affect the shape of $\overline{N}_\gamma(A)$ or $\overline{E}_\gamma(A)$, only the magnitudes.

The dependence of these photon observables on A is rather striking since they appear to be stronger functions of A than the measured neutron multiplicity as a function of fragment mass, $\overline{\nu}(A)$. Given the shape of the total kinetic energy dependence as a function of A_H , the neutron sawtooth could be easily reproduced with FREYA. However, our photon calculations are almost independent of both A and TKE, unlike our calculated $\overline{\nu}(A)$. This independence seems rather intuitive because by the time neutron emission ceases, the amount of excitation energy left in the fragment is below the neutron separation energy of several MeV and, apart from the odd-even effects, the neutron separation energy does not change strongly with A . The fragment deformation is probably not able to account for this strong dependence. If it were, photon emission would also be minimal at $A \approx 132$ where the doubly-closed neutron and proton shells result in a near-spherical heavy fragment but this is clearly not the

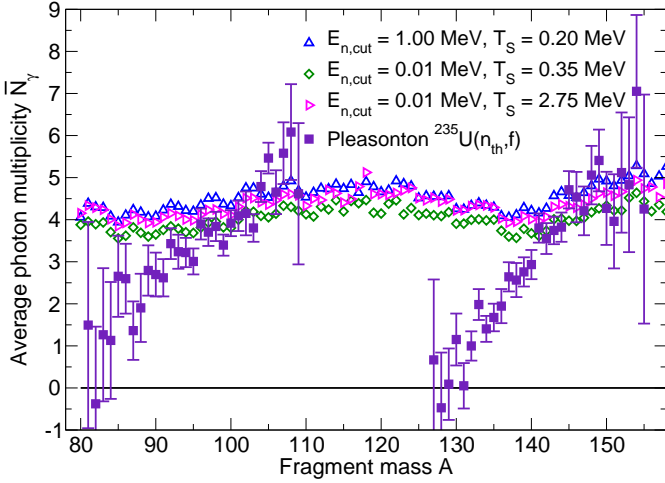


FIG. 11: (Color online) The average total photon multiplicity as a function of fragment mass compared to data from thermal neutron-induced fission of ^{235}U [5] (■). The calculations are $E_{n,\text{cut}} = 1$ MeV, $T_S = 0.20$ MeV (\triangle) and, with $E_{n,\text{cut}} = 0.01$ MeV, $T_S = 0.35$ MeV (\diamond) and 2.75 MeV (\triangleright).

case. Instead, the shape of the data would suggest a very strong A dependence of any competition between neutron and photon emission.

Finally we show the dependence of the photon energy on the fragment TKE for $^{235}\text{U}(n_{\text{th}},f)$ in Fig. 12. Again the calculations with $T_S = 0.35$ MeV lie significantly below the data, while the agreement with the other two calculations is considerably better. There is some characteristic curvature of the calculated \bar{E}_γ with TKE that is absent in the spontaneous fission results shown in Fig. 8.

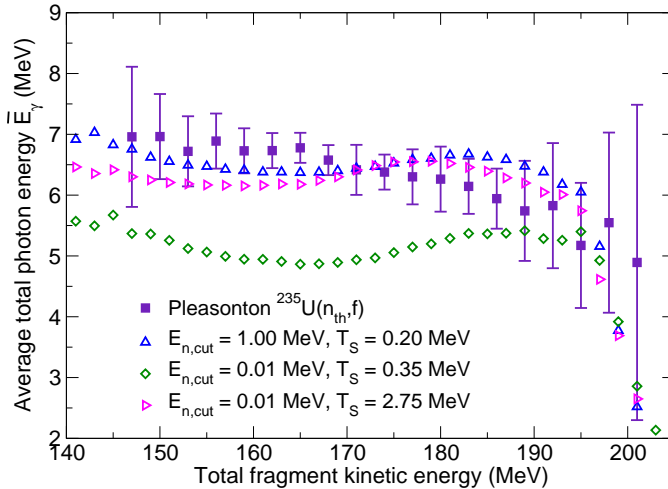


FIG. 12: (Color online) The average total photon energy emitted in a fission event as a function of the total fragment kinetic energy in the event compared to the data on thermal neutron induced fission of ^{235}U [5] (■). The calculations are $E_{n,\text{cut}} = 1$ MeV, $T_S = 0.20$ MeV (\triangle) and, with $E_{n,\text{cut}} = 0.01$ MeV, $T_S = 0.35$ MeV (\diamond) and 2.75 MeV (\triangleright).

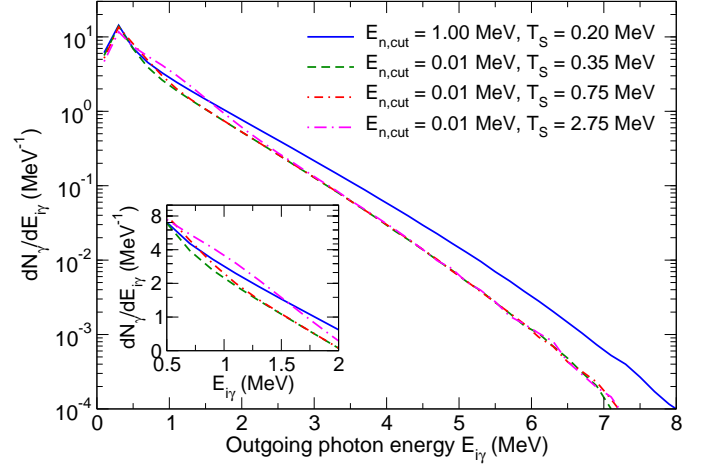


FIG. 13: (Color online) The calculated prompt fission photon spectrum from $^{252}\text{Cf}(sf)$ as a function of emitted single photon energy. The results are normalized to the total average multiplicity. The calculations show $E_{n,\text{cut}} = 1$ MeV, $T_S = 0.20$ MeV (solid) and, with $E_{n,\text{cut}} = 0.01$ MeV, $T_S = 0.35$ MeV (dashed), 0.75 MeV (dot-short-dashed), and 2.75 MeV (dot-long-dashed). The inset shows the difference between the calculations for $0.5 \leq E_\gamma \leq 2$ MeV.

C. Photon spectrum

Figure 13 shows the calculated spectral distribution of individual prompt photons emitted during the spontaneous fission of ^{252}Cf for several of the cases considered above. FREYA bins the energy of each emitted photon to generate the spectra shown in the figure. Figure 13 does not show all the cases we have studied because the high-energy behavior is the same for all values of T_S with $E_{n,\text{cut}} = 0.01$ MeV.

The only significant differences for fixed $E_{n,\text{cut}}$ occur for low photon energies, $E_{i\gamma} < 2$ MeV. Here, increasing T_S enhances the photon yield because the additional photon yield comes from yrast emission. The yrast photon yield increases by ≈ 1.0 for fixed $E_{n,\text{cut}}$ between $T_S = 0.20$ MeV and 2.75 MeV, while the statistical photon yield remains fixed. Since the yrast photons are emitted after the statistical emission of photons is complete in FREYA, the yrast photons are predominantly of low energy, causing the differences in the spectra highlighted in the inset of Fig. 13. We note, however, that an increase of T_S also increases the energy of the yrast photons by ≈ 1.3 MeV over the range of T_S studied.

On the other hand, increasing $E_{n,\text{cut}}$ increases the statistical photon yield by ~ 1.5 for fixed T_S in addition to increasing the average energy of the emitted photons by ~ 1.7 MeV. This results in the overall ‘hotter’ photon energy spectrum shown by the solid curve in Fig. 13.

Table IV shows the average single photon energies and their dispersion as well as the average energy and associated dispersion for the combined photon emission in a given event, both for $^{252}\text{Cf}(sf)$ and $^{235}\text{U}(n_{\text{th}},f)$. These av-

erages are taken over *all* fission events, without any cuts on fragment mass or kinetic energy. Thus the average total energy given in Table IV may not be identical to that obtained in Table III by averaging over regions of A or TKE. The relative width of the energy distribution is also smaller. In addition to providing the results for the total photon multiplicity, we show the average energies for three photon multiplicity ranges: $1 \leq N_\gamma \leq 5$; $6 \leq N_\gamma \leq 8$; and $9 \leq N_\gamma \leq 16$. The dispersions on the single-photon energies are quite large. Furthermore, because the peak in the photon multiplicity occurs at $\langle \bar{N}_\gamma \rangle \approx 7-9$, the relative dispersions in $E_{i\gamma}$ and E_γ are largest in the lowest N_γ bin.

D. Neutron-photon correlations

As previously discussed in Sect. II, the LiBerACE Collaboration studied the ratio of discrete photon lines emitted from two identified deformed even-even product pairs: $^{106}\text{Mo}+^{144}\text{Ba}$, with neutron multiplicity, ν , of two, and $^{106}\text{Mo}+^{142}\text{Ba}$, with $\nu=4$. They searched for a systematic shift of the centroids of the two corresponding photon multiplicity distributions indicative of either a correlation (forward shift) or anticorrelation (backward shift) of neutron and photon emission. Due to statistical uncertainties, their data were unable to determine any measurable shift of the photon multiplicity or energy distribution for $\nu=4$ relative to $\nu=2$.

Previously, Nifenecker *et al.* [3] extracted a positive correlation between neutron and photon multiplicities, shown in Fig. 2(b). While the LiBerACE data do not support this conclusion, neither do they support the relatively strong anticorrelation predicted by the early Monte Carlo calculation of Ref. [16]. Our result, shown in Fig. 14, also exhibits an anticorrelation, albeit not as strong as in Ref. [16]. Indeed, for every increase in ν for a given fission event, the average photon multiplicity, $\langle \bar{N}_\gamma \rangle$, decreases. This anticorrelation is independent of $E_{n,\text{cut}}$ and T_S , but it weakens for higher photon multiplicities. In addition, the neutron-gated photon multiplicity distributions are shifted to higher \bar{N}_γ , as shown in Fig. 14(a).

The LiBerACE data are compared to our calculations with $E_{n,\text{cut}} = 1$ MeV, $T_S = 0.20$ MeV and with $E_{n,\text{cut}} = 0.01$ MeV, $T_S = 2.75$ MeV in Fig. 14(b). The anticorrelation is weakest with the larger $E_{n,\text{cut}}$, giving only a small shift between $\nu = 2$ and 4. While there is a larger shift for $E_{n,\text{cut}} = 0.01$ MeV and $T_S = 2.75$ MeV, both calculations are in qualitative agreement with the data. We note that the data does seem to exclude the lower value of T_S which is shifted to lower photon multiplicities, $\langle \bar{N}_\gamma \rangle \approx 8$ instead of ≈ 9 . It is interesting that there thus seems to be some incompatibility of these data with the DANCE measurement [11]. However, it should be recalled that our results, as well as those of Ref. [16], are an average of many fragment pairs, not only the Mo+Ba channels. It would be worth trying to design follow-up measurements that can either accu-

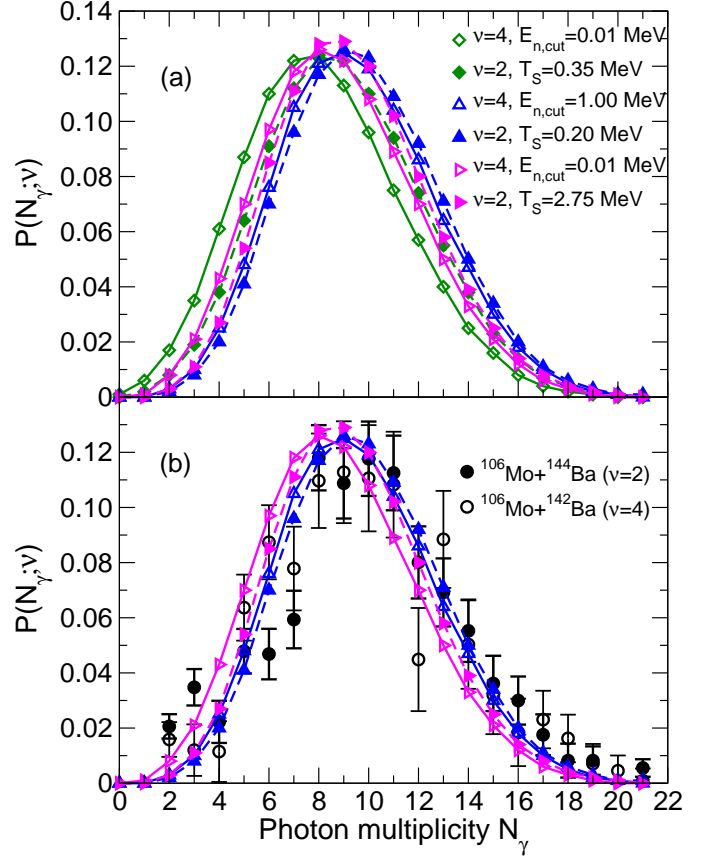


FIG. 14: (Color online) The photon multiplicity distribution gated on neutron multiplicity for $^{252}\text{Cf}(\text{sf})$. The results, averaged over all fragment masses, are shown in (a) for $E_{n,\text{cut}} = 1$ MeV, $T_S = 0.20$ MeV (\triangle) and with $E_{n,\text{cut}} = 0.01$ MeV, $T_S = 0.35$ MeV (\diamond) and $T_S = 2.75$ MeV (\triangleright). The neutron multiplicities are indicated by solid curves with filled symbols ($\nu=2$) and dashed curves with open symbols ($\nu=4$), e. g. (\blacktriangleright) and (\triangleright). Panel (b) shows the LiBerACE [13] data together with results calculated with $E_{n,\text{cut}} = 1$ MeV, $T_S = 0.20$ MeV (\triangle) and with $E_{n,\text{cut}} = 0.01$ MeV, $T_S = 2.75$ MeV (\triangleright).

mulate higher statistics for the Mo+Ba splits or study multiple lines with the same number of neutrons emitted (many pairs with $\nu = 2$ and $\nu = 4$) for a more direct comparison.

Figure 15 shows the angular correlation between two neutrons emitted from spontaneous fission of ^{252}Cf for neutrons with kinetic energies above a threshold of $E = 0.5, 1$ or 1.5 MeV. The angular modulation grows somewhat more pronounced as the threshold is raised (while the statistics are correspondingly reduced).

There is a significant forward-backward correlation, as discussed in detail in Ref. [2] before including the rotational component of the excitation energy. After adding E_{rot} , we find that the neutron correlations are unchanged for our low value of $E_{n,\text{cut}}$. The peak at $\theta_{12} = 0$ is due to both neutrons being emitted from the same fragment. The stronger correlation at $\theta_{12} = 0$ for larger threshold energies is due to the greater contribution to the correla-

T_S (MeV)	$E_{n,\text{cut}}$ (MeV)	N_γ bin	$\langle \overline{E}_{i\gamma} \rangle$ (MeV)	$\sigma_{\overline{E}_{i\gamma}}$ (MeV)	$\langle \overline{E}_\gamma \rangle$ (MeV)	$\sigma_{\overline{E}_\gamma}$ (MeV)
$^{252}\text{Cf}(\text{sf})$						
0.20	1.00	all	0.734	0.711	6.768	2.718
		$1 < N_\gamma < 5$	0.812	0.843	3.560	1.875
		$6 < N_\gamma < 8$	0.773	0.769	5.520	2.108
		$9 < N_\gamma < 16$	0.717	0.681	8.010	2.364
0.20	0.01	all	0.658	0.630	5.117	2.535
		$1 < N_\gamma < 5$	0.662	0.693	2.588	1.613
		$6 < N_\gamma < 8$	0.678	0.659	4.763	1.798
		$9 < N_\gamma < 16$	0.646	0.597	7.002	2.041
0.35	0.01	all	0.650	0.619	5.298	2.550
		$1 < N_\gamma < 5$	0.635	0.668	2.542	1.555
		$6 < N_\gamma < 8$	0.668	0.651	4.710	1.780
		$9 < N_\gamma < 16$	0.644	0.593	7.051	2.066
0.75	0.01	all	0.659	0.603	5.596	2.563
		$1 < N_\gamma < 5$	0.637	0.632	2.612	1.494
		$6 < N_\gamma < 8$	0.675	0.634	4.775	1.756
		$9 < N_\gamma < 16$	0.655	0.586	7.230	2.092
1.35	0.01	all	0.683	0.599	5.915	2.584
		$1 < N_\gamma < 5$	0.675	0.616	2.804	1.474
		$6 < N_\gamma < 8$	0.704	0.629	4.988	1.766
		$9 < N_\gamma < 16$	0.677	0.586	7.489	2.122
2.75	0.01	all	0.733	0.613	6.432	2.628
		$1 < N_\gamma < 5$	0.769	0.634	3.229	1.512
		$6 < N_\gamma < 8$	0.763	0.641	5.415	1.812
		$9 < N_\gamma < 16$	0.718	0.599	7.970	2.176
$^{235}\text{U}(n_{\text{th}},\text{f})$						
0.20	1.00	all	0.739	0.721	6.476	2.653
		$1 < N_\gamma < 5$	0.818	0.845	3.567	1.868
		$6 < N_\gamma < 8$	0.774	0.770	5.505	2.074
		$9 < N_\gamma < 16$	0.717	0.685	7.838	2.311
0.35	0.01	all	0.652	0.622	5.058	2.474
		$1 < N_\gamma < 5$	0.645	0.671	2.576	1.546
		$6 < N_\gamma < 8$	0.667	0.647	4.689	1.754
		$9 < N_\gamma < 16$	0.644	0.595	6.913	2.029
2.75	0.01	all	0.752	0.629	6.306	2.559
		$1 < N_\gamma < 5$	0.807	0.660	3.394	1.542
		$6 < N_\gamma < 8$	0.783	0.655	5.539	1.814
		$9 < N_\gamma < 16$	0.730	0.611	7.931	2.137

TABLE IV: The average single photon energy, $\langle \overline{E}_{i\gamma} \rangle$, and variance, $\sigma_{\overline{E}_{i\gamma}}$, as well as the average total photon energy, $\langle \overline{E}_\gamma \rangle$, and variance, $\sigma_{\overline{E}_\gamma}$, for the values of $E_{n,\text{cut}}$ and T_S considered. Results are shown for both $^{252}\text{Cf}(\text{sf})$ and $^{235}\text{U}(n_{\text{th}},\text{f})$.

tion from the emission of higher velocity neutrons from the light fragment. The peak at $\theta_{12} = 180$, due to the relative motion of the two fragments moving away from each other, arises when one neutron is emitted from each fragment. It is thus unaffected by the neutron energy threshold when $E_{n,\text{cut}}$ is negligible relative to the neutron threshold E . We present results for only one value of T_S in the top panel of Fig. 15 because the neutron correlation is essentially independent of T_S .

However, as $E_{n,\text{cut}}$ becomes comparable to E , the two-neutron correlation weakens. The effect is similar to that of increasing the average neutron multiplicity, *e.g.* for neutron-induced fission with incident energies above a few MeV: the correlation is reduced because it becomes more likely to emit more than one neutron from a single fragment. In this case, however, the increased value of $E_{n,\text{cut}}$ causes fragments with relatively low excitation energies to de-excite by photon emission rather than emit

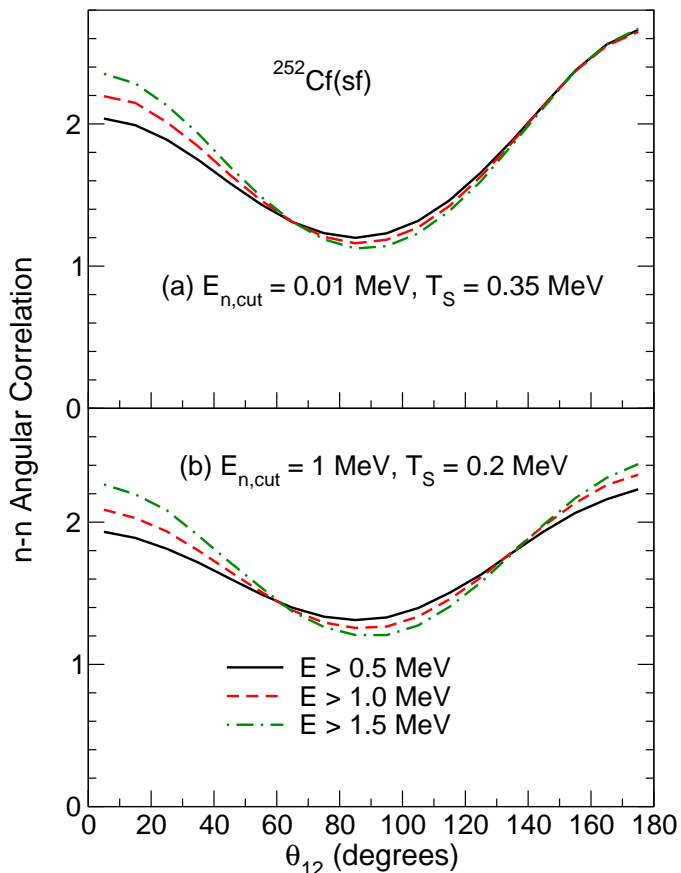


FIG. 15: (Color online) The angular correlation between two neutrons emitted in spontaneous fission of ^{252}Cf as a function of the opening angle between the two neutrons, θ_{12} . (a) Representative results for $E_{n,\text{cut}} = 0.01$ MeV, with $T_S = 0.35$ MeV. (b) The result for $E_{n,\text{cut}} = 1$ MeV and $T_S = 0.20$ MeV. The cuts on the neutron kinetic energy are $E > 0.5$ MeV (solid black), 1 MeV (dashed red), and 1.5 MeV (dot-dashed green).

another neutron. In this case, even if the two neutrons are emitted from different fragments, they are both affected equally by $E_{n,\text{cut}}$ so that the correlation at $\theta_{12} = 0$ is similar to that at $\theta_{12} = 180$.

There is no corresponding angular correlation between two photons because their high speed makes the effect of the Lorentz boosts imperceptible.

V. APPLICATIONS

Most of the measurements discussed have only studied gross features of photon emission, such as multiplicity and total energy. Modern detectors used to track and identify materials, however, would be better served by more sophisticated methods to better, more completely, characterize the materials of interest. In these, photons may be studied either in conjunction with neutron observables or alone, exploiting correlations, if possible.

The characteristic arrival of neutrons after photons in coincidence detectors can be a signature of fission in a material. Thus, fast detectors that can count and separate the prompt neutrons from prompt photon emission with typical energies of a few MeV could identify fissile material from the background. For example, the statistical distributions of neutrons are sensitive to the presence of fission chains in nuclear material [22, 23]. In principle, the photon multiplicity distribution encodes similar information [24]. However, the higher photon backgrounds make this information difficult to obtain in practice. Photon-neutron correlations may be the most likely place to look for such signatures. The new features of FREYA described here may make it possible to determine the conditions under which such signals can be extracted.

VI. CONCLUDING REMARKS

We have extended our event-by-event model of fission, FREYA, to photon emission and compared our calculations to the sometimes sparse available data on prompt fission photons. The data from the early 1970's yielding photon multiplicity and photon energy as functions of fragment mass and kinetic energy do not appear to be fully consistent with each other. The previous analyses are based on different assumptions regarding the relation between fragment excitation energy, deformation, and angular momentum which could lead to some of these inconsistencies. Data taken in the last few years have focused more on multiplicity distributions or spectra so that only the average multiplicity can be directly compared to the previous data and these appear to be somewhat higher on average than the previous results suggest. Clearly more data, taken with modern photon detectors, are needed. In particular, differential data with photon energy and multiplicity as a function of fragment mass and kinetic energy would be especially useful to make direct comparison to the earlier data of Refs. [3–5] and resolve their discrepancies.

Our calculations can rather successfully reproduce the recent DANCE measurement of the photon multiplicity distribution [12] albeit with a somewhat lower average angular momentum than suggested previously [10]. However, FREYA underestimates the previously reported measurements [3–5] of the average total energy of the emitted photons. Indeed, the earlier measurements obtained $\overline{E}_\gamma/\overline{N}_\gamma \approx 1$ MeV, while we find $\overline{E}_\gamma/\overline{N}_\gamma \approx 0.7$ MeV. Some of this discrepancy may be due to an incomplete understanding of the older detector setups. We have used the same detector threshold, $E_{\text{det}} = 0.15$ MeV, as in Ref. [11] for all our comparison calculations and the multiplicity is very sensitive to E_{det} .

We have tested the sensitivity of our results to the energy cutoff $E_{n,\text{cut}}$ below which photon emission dominates neutron emission; the choice of the spin temperature T_S governing the rotational energy; and the nuclear moment of inertia. We find that there is little sensitivity

of the neutron observables to any of these parameters, provided that the parameter $dTKE$ modulating the total kinetic energy shift is adjusted, except in cases where $E_{n,cut}$ is on the order of 1 MeV or larger. A change of T_S has a larger effect on the total photon energy than on the photon multiplicity, while the effect of modifying the fragment moment of inertia is small.

Finally, so far our calculations have assumed that there is essentially no competition between neutron and photon emission: neutron emission effectively ceases before photon emission begins. This lack of competition may be responsible for the failure to reproduce the sawtooth shape of the photon multiplicity and total energy as functions of fragment mass. Furthermore, only a single value of the spin temperature T_S was used, instead of an A

dependent value. Further model refinements will be introduced in future work as experiment allows.

Acknowledgments

We wish to acknowledge helpful discussions with A. Bernstein, D. L. Bleuel, D. A. Brown, A. Chyzh, C. Hagmann, E. B. Norman, and C.-Y. Wu. This work was supported by the Office of Nuclear Physics in the U.S. Department of Energy's Office of Science under Contracts No. DE-AC52-07NA27344 (RV) and DE-AC02-05CH11231 (JR).

-
- [1] M. B. Chadwick *et al.*, Nucl. Data Sheets **107** (2006) 2931.
 - [2] R. Vogt and J. Randrup, Phys. Rev. C **84**, 044621 (2011).
 - [3] H. Nifenecker, C. Signarbieux, M. Ribrag, J. Poitou, and J. Matuszek, Nucl. Phys. A **189**, 285 (1972).
 - [4] E. Nardi, A. Gavron, and Z. Fraenkel, Phys. Rev. C **8**, 2293 (1973).
 - [5] F. Pleasonton, R. L. Ferguson, and H. W. Schmitt, Phys. Rev. C **6**, 1023 (1972).
 - [6] V. F. Apalin, Yu. N. Gritsyuk, I. E. Kutikov, V. I. Lebedev, and L. A. Mikaelian, Nucl. Phys. A **71**, 553 (1965).
 - [7] G. J. Garvey, W. J. Gerace, R. L. Jaffe, I. Talmi, and L. Kelson, Rev. Mod. Phys. **41**, 51 (1969).
 - [8] M. M. Hoffman, Phys. Rev. **133**, B714 (1964).
 - [9] E. Nardi, L. G. Moretto and S. G. Thompson, Phys. Lett. B **43**, 258 (1973).
 - [10] J. B. Wilhelmy, E. Cheifetz, R. C. Jared, S. G. Thompson, H. R. Bowman, and J. O. Rasmussen, Phys. Rev. C **5**, 2041 (1972).
 - [11] A. Chyzh *et al.*, Phys. Rev. C **85**, 02160(R) (2012).
 - [12] M. Heil *et al.*, Nucl. Instr. Meth. A **459**, 229 (2001).
 - [13] D. L. Bleuel *et al.*, Nucl. Instr. Meth. A **624**, 691 (2010).
 - [14] C. Y. Wu *et al.*, Nucl. Instr. Meth. A **694**, 78 (2012).
 - [15] G. S. Brunson Jr., LA-940B-T (1982).
 - [16] S. Lemaire, P. Talou, T. Kawano, M. B. Chadwick, and D. G. Madland, Phys. Rev. C **72**, 014602 (2005).
 - [17] J. Randrup and R. Vogt, Phys. Rev. C **80**, 024601 (2009).
 - [18] O. Litaize and O. Serot, Phys. Rev. C **82**, 054616 (2010).
 - [19] R. Vogt, J. Randrup, D. A. Brown, M. A. Descalle, and W. E. Ormand, Phys. Rev. C **85**, 024608 (2012).
 - [20] C. Budtz-Jørgensen and H. H. Knitter, Nucl. Phys. A **490**, 307 (1988).
 - [21] H. R. Bowman, J. C. D. Milton, S. G. Thompson, and W. J. Swiatecki, Phys. Rev. **129**, 2133 (1963).
 - [22] R. P. Feynman, F. deHoffmann and R. Serber, J. Nucl. Ener. **3**, 64 (1956).
 - [23] N. Snyderman and M. Prasad, LLNL report UCRL-TR-218042 (2005).
 - [24] T. Gozani, ANS Trans. **24**, November 1976.